Nonequilibrium carrier-carrier scattering in two-dimensional carrier systems

Michael G. Kane
David Sarnoff Research Center, Princeton, New Jersey 08543
(Received 13 May 1996; revised manuscript received 26 August 1996)

Two-dimensional carrier-carrier scattering in GaAs is studied by means of calculations using the dynamically screened Boltzmann equation. We examine the dependence of scattering on density, and compare scattering in two-dimensional and three-dimensional systems. We also investigate the difference between dynamic and static screening models. To our knowledge these are the first calculations of two-dimensional carrier-carrier scattering using integration of the dynamically screened Boltzmann equation. [S0163-1829(96)04347-0]

I. INTRODUCTION

Studies of carrier-carrier scattering in three-dimensional (3D) semiconductor systems have reached a point where experiments and calculations are in good agreement. The situation in reduced-dimensionality systems is very different. Conclusive experimental studies are few, and calculations have not been as rigorous as in 3D. In quantum wells the experimental situation continues to be dominated by the experiments performed between 1986 and 1989 by Knox and co-workers.[1] Calculations of two-dimensional (2D) carrier-carrier scattering have not yet explored the dependence of scattering on relevant parameters such as the carrier density.

In this paper we extend our earlier study of 3D carrier-carrier scattering[2] to two dimensions. Nearly all previous calculations of 2D carrier-carrier scattering have used a static screening model.[3] To our knowledge the only exception is the Monte Carlo study by El-Sayed and Haug.[4] A static screening model can lead to nonphysical divergences in the 2D collision integral, while no such divergences can occur with a dynamic screening model.[5] Therefore we follow the same method employed in our earlier 3D study, using the full dynamic dielectric function, including the RPA carrier susceptibility and the Fröhlich lattice susceptibility. To our knowledge these are the first calculations of 2D carrier-carrier scattering using integration of the dynamically screened Boltzmann equation.

II. METHOD

A. 2D Boltzmann equation for Coulomb scattering

Our calculations model a 2D layer of carriers in GaAs, as occurs, for example, in a GaAs quantum well. For simplicity the material surrounding the layer of carriers is treated as having the same dielectric properties as the GaAs in which the carriers are confined. Since all the carriers are in a single layer, the calculations apply to single quantum wells, and to multiple-quantum-well structures where the wells are far enough apart that interactions between wells can be ignored.

The rate at which a carrier scatters out of a state with in-plane wave vector $\mathbf{k}_1$ due to each scattering process is

$$\left.\frac{\partial f(\mathbf{k}_1)}{\partial t}\right|_{\text{out}} = \frac{2\pi}{\hbar}\frac{g}{(2\pi)^4}\int d^2k_2\, d^2k_3\, d^2k_4\, |M(q,\omega)|^2 \times f(\mathbf{k}_1)f(\mathbf{k}_2)[1-f(\mathbf{k}_3)][1-f(\mathbf{k}_4)] \times \delta(\mathbf{k}_1+\mathbf{k}_2-\mathbf{k}_3-\mathbf{k}_4)\,\delta(E_1+E_2-E_3-E_4). \tag{1}$$

The in-plane wave vectors and energies of the initial states of colliding carriers 1 and 2 are $\mathbf{k}_1$, $\mathbf{k}_2$, E_1, and E_2, respectively, and $\mathbf{k}_3$, $\mathbf{k}_4$, E_3, and E_4 are the respective wave vectors and energies of their final states. The factor $g=2$ accounts for the degeneracy of k_2 states. An analogous equation describes the scattering into the state $\mathbf{k}_1$. The six-dimensional integral in Eq. (1) can be simplified by performing three of the integrals analytically, taking advantage of the effective-mass approximation, and the fact that the distribution function is isotropic in 2D k space. Three wave-number integrals remain, and converting two of these to energy integrals yields

$$\left.\frac{\partial N(E_1)}{\partial t}dE_1\right|_{\text{out}} = \frac{2\pi}{\hbar}\frac{g^2}{(2\pi)^6}\frac{2\pi m_1 m_2\sqrt{2m_2}}{\hbar^5}\frac{dE_1}{\sqrt{E_1}} \times \int_0^\infty \frac{dE_2}{\sqrt{E_2}}\int_0^\infty \frac{dE_3}{\sqrt{E_3}}\int_{q_{\min}}^{q_{\max}} dq\, |M(q,\omega)|^2 \times \left[1-\left(\frac{k_1^2+k_3^2-q^2}{2k_1k_3}\right)^2\right]^{-1/2} \times \left[1-\left(\frac{k_4'^2-k_2^2-q^2}{2k_2q}\right)^2\right]^{-1/2} f(E_1)f(E_2) \times [1-f(E_3)][1-f(E_4')], \tag{2}$$

where $N(E_1)dE_1$ is the areal density of carriers between E_1 and E_1+dE_1. The effective masses of carriers 1 and 2 are m_1 are m_2, respectively. By energy conservation $E_4'=E_1+E_2-E_3$, with k_4' the corresponding wave number. The wave-number limits correspond to the minimum and maximum in-plane momentum transfers, $q_{\min}=\max(|k_1-k_3|,|k_2-k_4'|)$ and $q_{\max}=\min(k_1+k_3,k_2+k_4')$.

We include electron-electron and electron-hole scattering processes, but only carriers in the lowest conduction subband

E_1 and the lowest valence subband HH_1 are considered. As a result the calculations are strictly valid only for quantum wells where the excited subbands are separated from the ground subbands by sufficiently large energies. Our calculations treat all bands as parabolic and isotropic, using scalar effective masses. The 2D electron mass is approximately the same as the 3D mass $m_e=0.067m_0$. In the diagonal approximation to the Luttinger matrix the in-plane mass in the heavy hole HH_1 subband is $m_{hh}=m_0/(\gamma_1+\gamma_2)$, where γ_1 and γ_2 are the first two Luttinger parameters. Taking the Luttinger parameters to be $\gamma_1=6.85$ and $\gamma_2=2.1$,[6–8] we obtain an in-plane mass $m_{hh}=0.11m_0$.[8] A more exact analysis that does not make the diagonal approximation gives the same result for narrow wells.[7]

The probability of a collision that transfers in-plane momentum $\hbar q$ and energy $\hbar\omega$ between two carriers is calculated from the square of the 2D Coulomb matrix element $M(q,\omega)=2\pi e^2F(q)/q\epsilon(q,\omega)$. Here $F(q)$ is a form factor to take into account the z component of the 3D Coulomb matrix element acting on the z dependence of the carrier wave functions. The form factor reduces the matrix element by less than 20% for $qd\leqslant 1$, where d is the well width. For the scattering calculations performed here, the range of important scattering wave vectors was found to be $q\leqslant 10^6$ cm^{-1}, so that for well widths $\leqslant 100$ Å the effect of the form factor is small. Therefore, for computational efficiency $F(q)$ is set to unity. This will lead to a small overestimate of the 2D scattering rate, but there is a compensating overestimate of the screening that results from setting $F(q)=1$ in the calculation of the dielectric function.

The combination of using the narrow-well limit and neglecting the effects of the excited subbands is a consistent use of the quantum limit. It is expected that the effects of quantum confinement will be strongest in the quantum limit, and that corrections to the quantum limit for finite well widths will modify the results in the direction of 3D behavior.

B. Dielectric function for 2D carriers

The longitudinal random-phase-approximation (RPA) dielectric function in the plane of the carriers is

$$\epsilon(\mathbf{q},\omega)=\epsilon_\infty+\frac{\omega_{TO}^2(\epsilon_0-\epsilon_\infty)}{\omega_{TO}^2-\omega^2-i\gamma\omega}+2\pi\beta\sum_i \chi_i(\mathbf{q},\omega), \quad (3)$$

where $\beta^2=q^2-\epsilon_\infty\omega^2/c^2$. The first two terms represent the 3D frequency-dependent Fröhlich lattice susceptibility, using standard values for the lattice parameters ϵ_0, ϵ_∞, ω_{TO}, and γ.[9] The last term represents the contribution from the 2D carrier dielectric susceptibilities $\chi_i(\mathbf{q},\omega)$. For our calculations the very good approximation $\beta=q$ is used. As noted, only the E_1 and HH_1 subbands are included, so that i ranges over only these two subbands.

Just as the quantum limit is applied in the treatment of the Boltzmann equation, so also in the calculation of the carrier susceptibilities. The general form for the RPA susceptibility of carriers of type i is

$$\chi_i(\mathbf{q},\omega)=\frac{e^2}{q^2}\int\frac{d^2k}{2\pi^2}\frac{f_i(\mathbf{k})-f_i(\mathbf{k}+\mathbf{q})}{\hbar\omega+E_i(\mathbf{k}+\mathbf{q})-E_i(\mathbf{k})+i\delta}, \quad (4)$$

where $f_i(\mathbf{k})$ is the occupation probability of the state with in-plane wave vector $\mathbf{k}$. Causality is enforced in the retarded dielectric function by making δ a small positive quantity, thereby placing all poles in the lower half of the complex ω plane. Using the effective-mass approximation $E_i(k)=\hbar^2k^2/2m_i$, where m_i is the effective mass of a carrier of type i, the angular integration in Eq. (4) can be performed analytically, and the remaining k integration can be converted to an energy integration, yielding[5]

$$\begin{aligned}\chi_i(q,\omega)=\frac{m_ie^2}{\pi\hbar^2q^2}\int dE\ f_i(E)\\ \times\{[\hbar\omega+\hbar^2kq/m_i+E_i(q)+i\delta]^{-1/2}\\ \times[\hbar\omega-\hbar^2kq/m_i+E_i(q)+i\delta]^{-1/2}\\ -[\hbar\omega+\hbar^2kq/m_i-E_i(q)+i\delta]^{-1/2}\\ \times[\hbar\omega-\hbar^2kq/m_i-E_i(q)+i\delta]^{-1/2}\}. \quad (5)\end{aligned}$$

III. RESULTS OF CALCULATIONS

A. Density dependence

To investigate the density dependence of 2D carrier-carrier scattering, calculations were performed at plasma densities from 10^9 to 5×10^{11} cm^{-2}. We model an experiment in which 2D electron-hole pairs are generated in GaAs with an average electron energy of 20 meV, and an average hole energy of 12 meV. The initial energy width of the electron peak is 20 meV (full width at half maximum). These parameters correspond to the conditions in the experiments of Knox and co-workers on undoped quantum wells.[1]

Figure 1 shows the evolution of the electron distribution at the different densities. Modeling the initial scattering rate (based on the rate at which the peak height drops) as proportional to N^α, where α can be density dependent, we find that $\alpha=0.91$ at densities between 10^9 and 10^{10} cm^{-2}. Thus at low densities the scattering rate increases nearly linearly with the 2D plasma density, in agreement with experiments by Kash on 2D scattering of hot carriers in an equilibrium distribution.[10] At higher densities the increase becomes strongly sublinear due to the effects of screening and Pauli suppression of scattering among states near the peak, which is included by the final-state Fermi factors $(1-f_e)$ in the Boltzmann equation. Thus $\alpha=0.60$ between $N=10^{10}$ and 5×10^{10} cm^{-2}, and $\alpha=0.24$ between $N=5\times10^{10}$ and 10^{11} cm^{-2}. At higher densities the carrier-carrier scattering actually begins to decrease with density, so that at 5×10^{11} cm^{-2} the scattering is significantly slower than at 10^{11} cm^{-2}. The reduced scattering at high densities is due to Pauli exclusion. For the initial electron distribution used here, at a density of 5×10^{11} cm^{-2} the occupation probability at the peak is $f_e=0.85$, so that it is reasonable for the scattering rate to decrease with density. It was found that when the Fermi factors are omitted from the calculation, the scattering rate continues to increase with density.

The results of our calculations can be compared with the experimental results of Knox and co-workers. They investigated densities of 2×10^{10} and 5×10^{11} cm^{-2} in undoped GaAs quantum wells. At a density of 2×10^{10} cm^{-2}, their results showed that after 150 fs the spectral peak has dropped

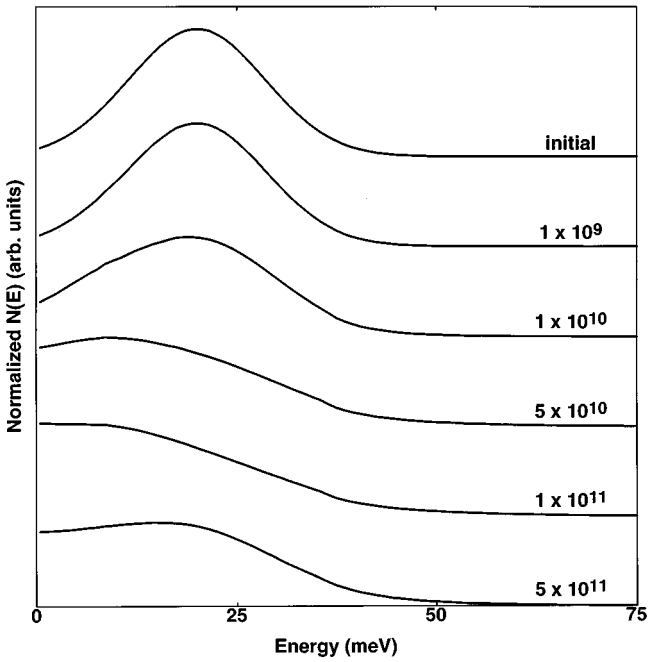

FIG. 1. The initial and final electron energy distribution in photoexcited 2D plasmas at densities from 10^9 to 5×10^{11} cm^{-2}, as calculated by integrating the dynamically screened Boltzmann equation for 150 fs. The distributions are normalized to the total density, and the baseline for each plot can be determined from the right-hand edge of the figure.

but is still visible, and it has shifted down in energy. An interpolation between our calculated results for 10^{10} and 5×10^{10} cm^{-2} yields the same behavior, with a peak in the electron distribution still present after 150 fs, but diminished in height and shifted down in energy toward the subband edge due to cooling by holes. At a density of 5×10^{11} cm^{-2}, Knox and co-workers observed that the spectral peak lasted only for the duration of the 100-fs optical pulse. As shown in Fig. 1, the calculations at $N=5\times10^{11}$ cm^{-2} indicate that, even after 150 fs, a diffuse spectral peak should still be observed. However, the density in the experiment was probably lower than 5×10^{11} cm^{-2}, since this density would correspond to $f_e+f_h=1.7$ at the peak, which cannot be achieved by incoherent excitation. At $N=10^{11}$ cm^{-2} the calculated scattering is indeed more rapid, removing the spectral peak after about 100 fs. We find that the scattering is fastest at $N=3\times10^{11}$ cm^{-2}, which is the maximum density achievable in GaAs by incoherent optical excitation with these energy parameters, since $f_e=f_h=0.5$ at the peak. It is reasonable that this density yields the most rapid scattering, since the product $f_e(1-f_e)$ occurring in the Boltzmann equation is maximized for $f_e=0.5$. Thus our calculations are in qualitative agreement with the high-density experiment of Knox and co-workers, if we assume that the plasma density in this experiment was actually in the range of $1–3\times10^{11}$ cm^{-2}.

B. Comparison of 2D and 3D scattering

We performed calculations comparing 2D and 3D carrier-carrier scattering at densities related by $N=n^{2/3}$. The results show that 2D scattering is more rapid than 3D scattering.

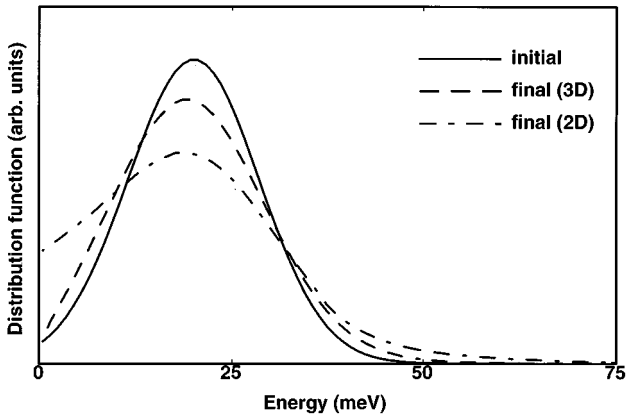

FIG. 2. A comparison of 2D and 3D electron-electron scattering. The final electron distributions are shown after 150 fs. The 3D calculation is performed at a density of 10^{16} cm^{-3}, and the 2D calculation at a density of 5×10^{10} cm^{-2}.

One reason is the presence of holes in the HH_1 subband with an effective mass that in GaAs is well matched to the electron mass in the E_1 subband. Our choice of GaAs as a material system is partly responsible for the match, and varying degrees of mass matching are to be expected in other materials. Furthermore, our use of the quantum limit is to some extent responsible for the matching of the masses. The hole mass in the HH_1 subband increases as the well width increases, due to repulsion between the HH_1 subband and the first excited subband. Therefore for finite well widths holes are expected to become less important for electron scattering, approaching the 3D result as the well width increases. An additional factor that decreases the 3D scattering rate is the presence of electrons excited from the light-hole band, skewing the electron distribution toward lower energies, and thus slightly enhancing the screening.

To examine the effect of dimensionality alone on carrier-carrier scattering, calculations were performed on a single-peak electron distribution without the presence of holes in 2D and 3D. The 2D and 3D densities are 5×10^{10} and 10^{16} cm^{-3}, which are related as $N=n^{2/3}$. Figure 2 shows the results. Even in the absence of holes, and without lower-energy electrons skewing the 3D distribution, the initial 2D carrier-carrier scattering rate is 2.8 times more rapid than the 3D rate. We attribute the difference to the weaker screening that occurs in 2D compared to 3D because of the restricted motion of the 2D carriers. It is also possible that the more rapid 2D scattering is partially due to differences in the bare Coulomb interaction, which yields a $1/q^2$ dependence of the squared matrix element in 2D, and $1/q^4$ in 3D. Indeed, the two effects—the different bare interaction and the different screening—might be difficult to disentangle.

C. Dynamic vs static screening

To investigate the difference between the predictions of dynamic and static screening models in 2D, calculations were performed using the 2D static RPA dielectric function $\epsilon(q,0)$, obtained by setting $\omega=0$ in Eq. (3). The statically screened scattering rate for a 2D photoexcited distribution

diverges in a nonphysical manner in the limit of small momentum transfers.[5] Therefore dynamic and static screening models cannot be compared for the case of scattering in the absence of a background plasma. To compare the two screening models we simulate photoexcited carriers scattering in a 100-K equilibrium background. The total plasma density is 5×10^{10} cm^{-2}, of which 80% is the background carriers and 20% is a 50-meV nonequilibrium distribution having the same parameters as used for previous calculations, with appropriate hole energies.

Results for the two screening models are shown in Fig. 3. The static screening model underestimates the scattering rate by a factor of approximately 3, demonstrating the importance of using a dynamic screening model in calculations of 2D carrier-carrier scattering.

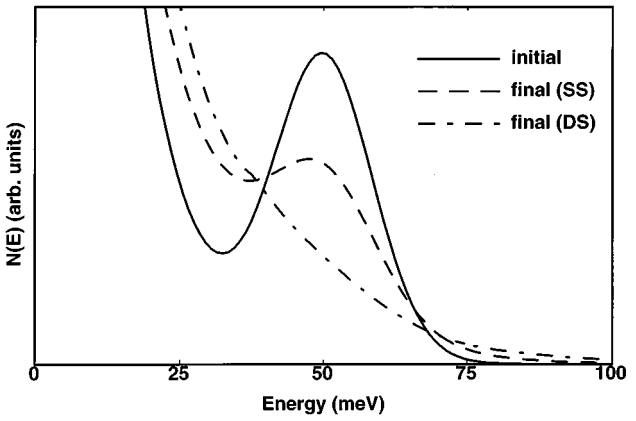

FIG. 3. A comparison of static screening (SS) and dynamic screening (DS) models for scattering of photoexcited carriers in a cool plasma background for 150 fs. The total plasma density is 5×10^{10} cm^{-2}, of which a hot nonequilibrium plasma makes up 20%, with the rest made up of a 100-K equilibrium plasma.

IV. CONCLUSION

We performed dynamically screened calculations of 2D carrier-carrier scattering in GaAs. At densities below 10^{10} cm^{-2} the scattering rate increases nearly linearly with density, but at higher densities the increase becomes strongly sublinear due to the effects of screening and Pauli exclusion. It was also found that carrier-carrier scattering is more rapid in 2D than in 3D, assuming densities that are related by $N=n^{2/3}$. Static and dynamic screening models were compared using calculations of energetic 2D carriers scattering in a cool equilibrium background. The two models were found to yield different results, just as they do in 3D, with the static screening model significantly underestimating the scattering rate. Our results indicate that it is important for a dynamic screening model to be used in calculating 2D carrier-carrier scattering.

[1] W. H. Knox, C. Hirlimann, D. A. B. Miller, J. Shah, D. S. Chemla, and C. V. Shank, Phys. Rev. Lett. **56**, 1191 (1986); W. H. Knox, D. S. Chemla, G. Livescu, J. E. Cunningham, and J. E. Henry, *ibid.* **61**, 1290 (1988); W. H. Knox, Solid-State Electron. **32**, 1057 (1989).

[2] M. G. Kane, K. W. Sun, and S. A. Lyon, Phys. Rev. B **50**, 7428 (1994).

[3] Calculations of 2D carrier-carrier scattering using a static screening model can be found in D. W. Bailey, M. A. Artaki, C. J. Stanton, and K. Hess, J. Appl. Phys. **62**, 4638 (1987); C. J. Stanton, D. W. Bailey, and K. Hess, IEEE J. Quantum Electron. **24**, 1614 (1988); Phys. Rev. Lett. **65**, 231 (1990); S. M. Goodnick and P. Lugli, Appl. Phys. Lett. **51**, 584 (1987); Solid-State Electron. **31**, 463 (1988); Phys. Rev. B **37**, 2578 (1988); **38**, 10 135 (1988); S. M. Goodnick, P. Lugli, W. H. Knox, and D. S. Chemla, Solid-State Electron. **32**, 1737 (1989); C. Kiener, G. Zandler, and E. Vass, Solid-State Commun. **65**, 1241 (1988); P. J. van Hall and P. W. M. Blom, Superlatt. Microstruct. **13**, 329 (1993); V. Cambel and M. Moško, Semicond. Sci. Technol. **9**, 474 (1994); M. Moško and A. Mošková, *ibid.* **9**, 478 (1994).

[4] K. El Sayed and H. Haug, Phys. Status Solidi B **173**, 189 (1992).

[5] M. G. Kane, Ph.D. thesis, Princeton University, 1994.

[6] H. Haug and S. W. Koch, *Quantum Theory of the Optical and Electronic Properties of Semiconductors*, 2nd ed. (World Scientific, Singapore, 1993).

[7] G. Bastard, *Wave Mechanics Applied to Semiconductor Heterostructures* (Halsted, New York, 1988).

[8] L. J. Sham, in *Physics of Low-Dimensional Semiconductor Structures*, edited by P. Butcher, N. H. March, and M. P. Tosi (Plenum, New York, 1993).

[9] J. S. Blakemore, J. Appl. Phys. **53**, R123 (1982).

[10] J. A. Kash, Phys. Rev. B **48**, 18 336 (1993).